FOUNTAIN JOURNAL OF NATURAL & APPLIED SCIENCES

A Publication of the College of Natural & Applied Sciences

Fountain University, Osogbo, Nigeria

Synthesis and characterisation of electrospun ZnO-TiO_2 mixed oxide nanofibrous film

Bolarinwa, H. S.[1]*, Animasahun, L. O[1], Onuu, M. U[2], Fasasi, A. Y[3]. Alayande, S. O.[4]

[1] Department of Physics, Electronics and Earth Sciences, Fountain University, Osogbo
[2] Alex Ekwueme Federal University, Ndufu-Alike
[3] Centre for Energy and Research Development, Obafemi Awolowo University, Ile-Ife
[4] Abiola Ajimobi Technical University, Ibadan, Oyo State

*Correspondence: babdulhakeem@gmail.com

ABSTRACT

This study investigates the effects of TiO_2 concentration on the optical and dielectric properties of ZnO electrospun nanofiber thin films, with the aim of enhancing visible-light absorption and conversion efficiency. Electrospun solutions of titanium(iv) propoxide, zinc acetate dihydrate, poly(vinyl acetate), and N, N-dimethylformamide were deposited onto glass substrates and subsequently calcined. The resulting fibres had a mean width of approximately 250 nm. Structural and optical characterisation using SEM, EDS, RBS, XRD, and UV–Vis spectroscopy revealed no significant lattice interaction between Zn and Ti atoms, while optical analysis indicated a redshift in the absorption edge and narrowing of the bandgap from 2.89 eV (5% Ti) to 2.39 eV (25% Ti). Urbach tail analysis demonstrated reduced disorder with higher Ti content. The dielectric and optical conductivity parameters increased with photon energy, particularly around the bandgap region. This work highlights a facile and reproducible electrospinning route for tailoring ZnO–TiO_2 nanofibres towards efficient visible-light photocatalysis and other optoelectronic applications.

ARTICLE INFO

Article history:
Received July 2025
Revised September 2025
Accepted September 2025

Keywords:
Photocatalyst, Visible light, Optical properties, Bandgap narrowing

Introduction

Zinc oxide (ZnO) and titanium dioxide (TiO_2) are widely studied materials due to their unique optical, chemical, and structural combination. ZnO is particularly attractive because of its one-dimensional (1D) nanomaterials, which can be fabricated using various deposition techniques [1]. The synthesis of ZnO-TiO_2 mixed oxide materials has gained significant attention recently due to their enhanced properties and versatile applications. Combining ZnO and TiO_2 can lead to synergistic effects, such as improved photocatalytic activity, enhanced stability, and increased surface area [2]. The synthesis of ZnO-TiO_2 mixed oxide materials can be achieved through various techniques. One such technique is electrospinning, which involves the production of 1D electrospun fibres consisting of different polymers [3]. Electrospinning offers a versatile and cost-effective method for fabricating ZnO-TiO_2 mixed oxide materials with controlled morphology and composition [4]. Due to their unique properties and potential applications, ZnO-TiO_2 electrospun mixed oxide nanofibers have gained significant attention in various fields. Incorporating nanosized oxides in catalyst formulations has enhanced long-term durability [5]. The use of electrospinning eliminates

DOI: https://doi.org/10.53704/fujnas.v14i1.980

the need for additional compatibilisers, as the polymer matrix itself can act as a mediator for in situ synthesis of nanostructured ZnO clusters [4, 6]. The applications of ZnO-TiO_2 mixed oxide materials are diverse and span different fields. One important application is environmental remediation, where these materials can remove agro-pollutants from soil and water [7]. The agricultural sector is a significant source of pollutants, such as mineral fertilisers and pesticides, which can harm the environment [8]. ZnO-TiO_2 mixed oxide materials have shown promising results in the remediation of these pollutants, contributing to environmental protection [8]. Another significant application of ZnO-TiO_2 mixed oxide materials is photocatalysis. In photocatalysis, TiO_2/ZnO nanofibers have shown higher photocatalytic properties than pure TiO_2 nanofibers [9]. These materials exhibit excellent photocatalytic properties, making them suitable for degrading organic compounds under UV and visible light irradiation [10]. The mixed anatase/rutile phase of TiO_2 in the mixed oxide system enhances the charge separation and improves the overall photocatalytic efficiency [11]. ZnO-TiO_2 mixed oxide materials are highly effective in mineralising different organic compounds under diffusion-controlled conditions [10]. Combining ZnO and TiO_2 in mixed-oxide systems can yield synergistic effects and improved performance compared to the individual materials [12]. The controlled synthesis of these materials, using techniques such as electrospinning, allows tailoring their properties to meet specific application requirements [4]. The rationale for modifying ZnO with TiO_2 lies in the uniqueness of ZnO-TiO_2 mixed oxide materials in terms of their tailored properties and the ability to control their composition and morphology.

Furthermore, the environmental and energy-related applications of ZnO-TiO_2 mixed oxide materials address critical challenges in sustainability and pollution control [13]. By tuning the synthesis parameters, such as the ratio of ZnO to TiO_2 and the calcination conditions, the properties of the mixed oxide materials can be optimised for specific applications [14].The synthesis of ZnO-TiO_2 mixed oxide materials, mainly through electrospinning, offers a versatile and cost-effective approach to fabricating materials with enhanced properties. This study stands out from other published works by demonstrating a reduction in the optical bandgap with increasing TiO_2 concentration, thereby improving the material's suitability for visible-light photocatalysis applications.

Material and method

Solution preparation: Titanium(iv) propoxide ($Ti(OC_3H_7)_4$), zinc acetate dihydrate ($Zn(CH_3COO)_2{\cdot}2H_2O$), poly(vinyl acetate) (PVAc), and N, N-dimethylformamide (DMF) were obtained from Sigma-Aldrich and used as received. Precursor mixtures with Zn: Ti ratios of 95:5, 85:15, and 75:25 were prepared. Two grams of the precursor mixture was dissolved in 1.6 g of PVAc solution in 20 mL of DMF, and the mixture was stirred until homogeneous.

Electrospinning process: The precursor solution was loaded into a syringe pump and electrospun for 3 h at a flow rate of 0.5 mL/h under 12 kV potential difference, with a tip-to-collector distance of 20 cm, ambient humidity of ~50%, and temperature of 25 °C. Glass substrates were pre-cleaned with dilute ethanol, hydrochloric acid, and distilled water. The collected fibres were calcined in a tubular furnace at 500 °C for 3 h.

Characterisation techniques: The surface morphology and elemental composition were analysed by scanning electron microscopy (SEM) and energy-dispersive X-ray spectroscopy (EDS). Film thickness and stoichiometry were measured using Rutherford backscattering spectroscopy (RBS). Structural properties were probed by X-ray diffraction (XRD), while optical characteristics, including transmittance, absorbance, and bandgap, were determined using UV–Vis spectroscopy. Optical constants (refractive index, extinction coefficient, dielectric constant, and optical conductivity) were calculated from the measured spectra.

Results

Morphology and elemental analysis

Figure 1 shows the SEM image of the ZnO-TiO_2 sample. The qualitative elemental composition of the samples was probed with energy-dispersive spectroscopy attached to the SEM. Figure 2 shows the EDS spectra for the selected 95% Zn to 5% Ti sample.

Rutherford backscattering spectroscopy (RBS)

The EDS results are supplemented by RBS analysis of the 75%Zn to 25%Ti sample (Figure 3) to further confirm the presence of the desired elements and determine the average fibre film thickness, an important parameter that affects many properties of thin solid structures of functional materials. Notably,

DOI: https://doi.org/10.53704/fujnas.v14i1.980

the film thickness is required for in-depth analysis of our optical and electrical data.

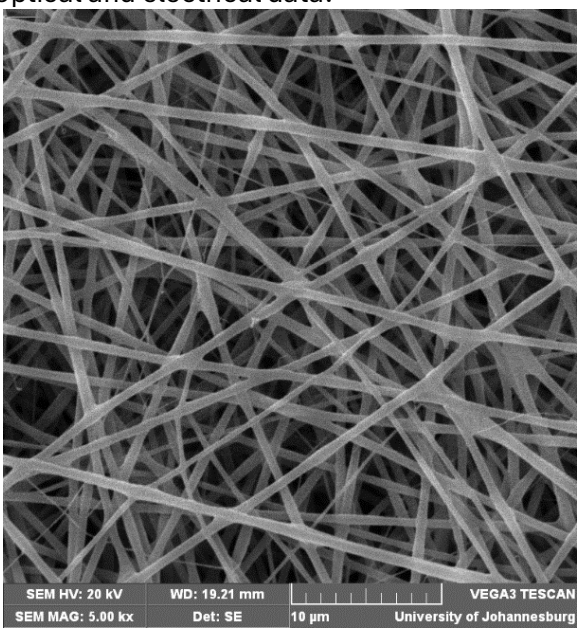

Figure 1: SEM Image of the ZnO-TiO_2 nanofibre

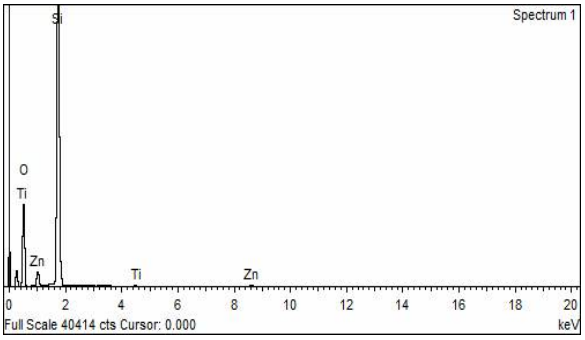

Figure 2. Energy dispersive X-ray (EDX) of calcined 95% Zn and 20% TiO_2 nanofibre

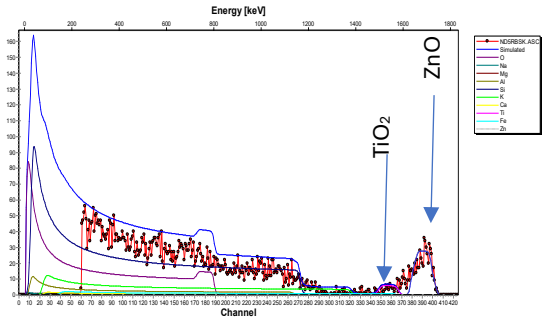

Figure 3. Rutherford Backscattering (RBS) spectrum of the calcined 75% ZnO and 25% TiO_2 electrospun nanofibre.

The stoichiometric ratios of the elements and the thickness (in atoms/cm2) of each sample were determined by RBS data simulations using the SIMNRA software. By dividing the thickness (in atoms/cm2) from the RBS analysis by the atomic density (in atoms/cm^3), then converting the result to nanometers (nm), one can compute the thickness in nanometers. The atomic density was estimated according to Equation 1 [15].

$$Atomic\ density = \frac{\rho N_a}{M} \qquad 1$$

where M is the molecular mass of the element, N_a is Avogadro's number, and ρ is the element's density. The atomic density of a compound or composite, such as a metal oxide, was determined by dividing the atomic density of each element by the fractional amount of that element present in the material and adding the results, as expressed in equation 2, and the result is presented in Table 1.

$$Thickness\ (nm) = \frac{thickness\ (atoms/cm^2) \times 10^7}{atomic\ density\ (atoms/cm^3)} \qquad 2$$

Table 1. Elemental concentration and thickness of the 75% ZnO and 25% TiO_2 electrospun nanofiber composite from RBS after simulation

Elements	Concentration	Thickness (atm/cm²)	Thickness (nm)
Zn	0.115040		
O	0.839421	1.16E+18	1142.607
Ti	0.045539		

X-ray Diffraction analysis

Figure 4 depicts the X-ray diffraction pattern for the composite nanofibre samples with the corresponding Miller indices for the ZnO and TiO_2 composite.

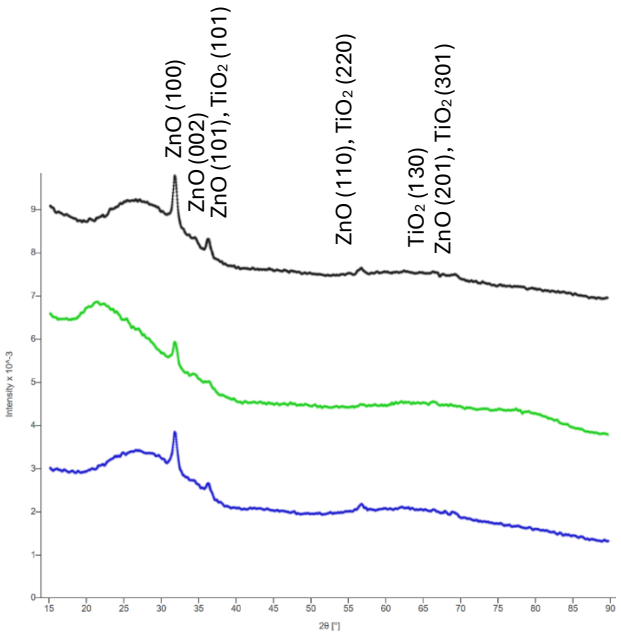

Figure 4. The XRD spectra of the calcined ZnO- TiO_2 nanofibre composite for the different compositions

DOI: https://doi.org/10.53704/fujnas.v14i1.980

Optical analysis

Transmittance, absorbance and the bandgap

Figures 5 and 6 show the transmittance and absorbance spectra of the ZnO – TiO_2 mixed oxide nanofibre. The Tauc Plot given in equation 3 was used to determine the optical bandgap of the ZnO-TiO_2 electrospun nanofiber composite. A plot of $(\alpha hv)^n \; against \; hv$ gives the Tauc plot for determining the bandgap; the resulting graph is shown in Figure 7.

$$\alpha = A\frac{(hv-E_g)^n}{hv} \qquad 3$$

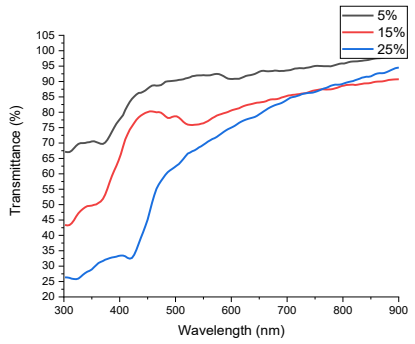

Figure 5 Transmission spectra of calcined ZnO-TiO_2 electrospun nanofibre

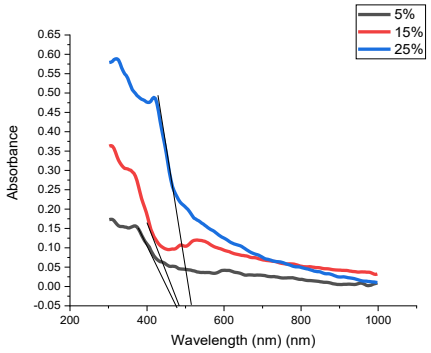

Figure 6. Absorbance spectra of calcined ZnO-TiO_2 electrospun nanofibre

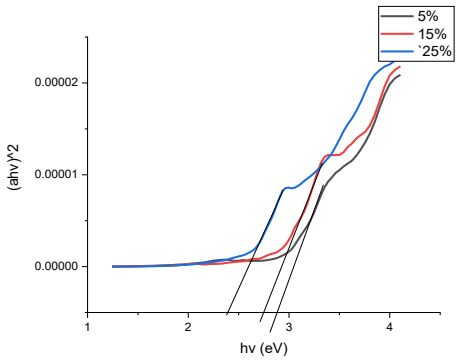

Figure 7. The plot of photon energy for the allowed direct bandgap ZnO-TiO_2

Tail width of localised states

Amorphous materials produce localised states stretched in the bandgap, which is why the exponential tail arises [16, 17]. Equation 4's Urbach rule is believed to govern the spectral dependence of the absorption edge at low photon energies.

where α_o is a constant, hv is the photon energy and ΔE denotes "the width of the tail of localised states in the bandgap" (Urbach energy).

$$\propto (v) = \alpha_o exp\left(\frac{hv}{\Delta E}\right) \qquad 4$$

By plotting ln(α) against hv, the reciprocal of the slope from the linear fit of the linear portions of the curves gives the Urbach tail width energy of the localised state of the bandgap (Figure 8). Table 2 shows that the localised states decrease with increased TiO_2 concentration.

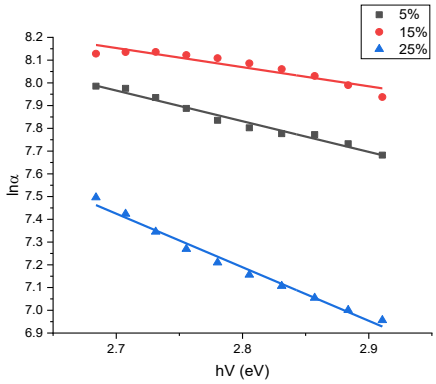

Figure 8. Plot showing the variation of lnα against photon energy for the ZnO-TiO_2 nanofibre

Table 2. Ubarch tail width for the calcine electrospun nanofibre

Samples	ΔE (meV)
ZnO-TiO_2 (95%Zn, 5%Ti)	1190
ZnO-TiO_2 (85%Zn, 15%Ti)	740
ZnO-TiO_2 (75%Zn, 25%Ti)	424

Refractive index and Extinction coefficient

Semiconducting materials' refractive index significantly affects their electrical and optical properties [18]. Materials with high refractive indices are known to capture incident rays [19]. To calculate this crucial semiconductor parameter, the reflectance was calculated theoretically using Equation 5 [20].

$$R = \sqrt{1-\frac{T}{\exp(-A)}} \qquad 5$$

where T is the transmittance, R is the reflectance, and A is the absorbance.

The plot of reflectance against wavelength for all the samples is presented in Figure 9. The refractive

DOI: https://doi.org/10.53704/fujnas.v14i1.980

index as a function r(λ) was then determined using equation 6. The result is presented in Figure 10.

$$n = \frac{1+\sqrt{R}}{1-\sqrt{R}} \quad 6$$

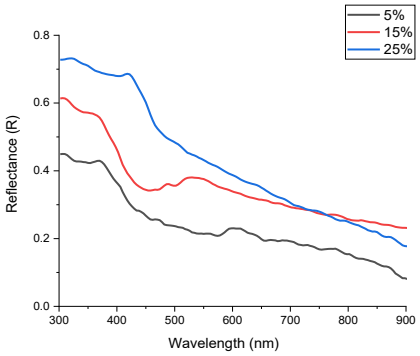

Figure 9. Reflectance spectra of calcined ZnO-TiO_2 electrospun nanofibre

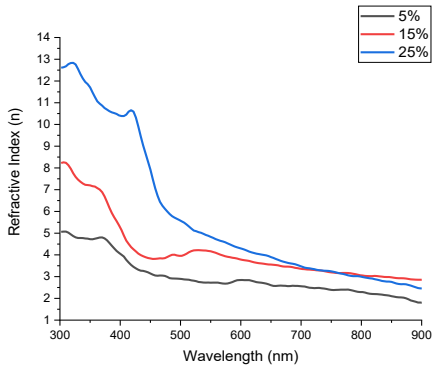

Figure 10. Refractive index spectra of calcined ZnO-TiO_2 electrospun nanofibre

The material characteristic, the extinction coefficient (k), defined by equation 11 and shown in Figure 11, indicates the degree to which a material absorbs light at a given wavelength. A material's refractive index of light dispersion has an impact on its extinction coefficient as well [21]. Equation 5 provides information about this relation.

$$k = \frac{\alpha\lambda}{4\pi} \quad 7$$

where k is the extinction coefficient, α= absorption coefficient, and λ is the wavelength. electrospun nanofiber

Dielectric and optical properties

The real and imaginary components of the dielectric constant of nanofibre materials can be determined from the material's extinction coefficient and refractive index. Equation 8 contains the relationship used.

$\varepsilon_r = n^2 - k^2$; $\varepsilon_i = 2nk$ 8

where n, k, εr, and εi stand for the refractive index, extinction coefficient, real dielectric constant, and nanofiber dielectric properties, which are represented by their respective characteristic curves in Figures 12 and 13.

imaginary dielectric constant, respectively. The real and imaginary parts of the ZnO-TiO_2 electrospun

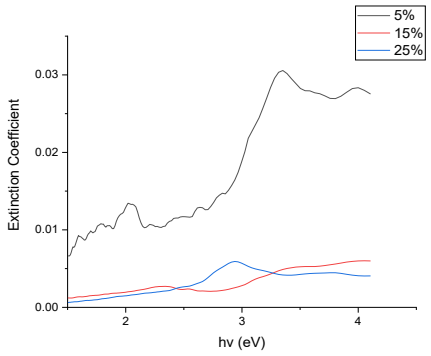

Figure 11. Graph of the extinction coefficient against the photon energy for ZnO–TiO_2

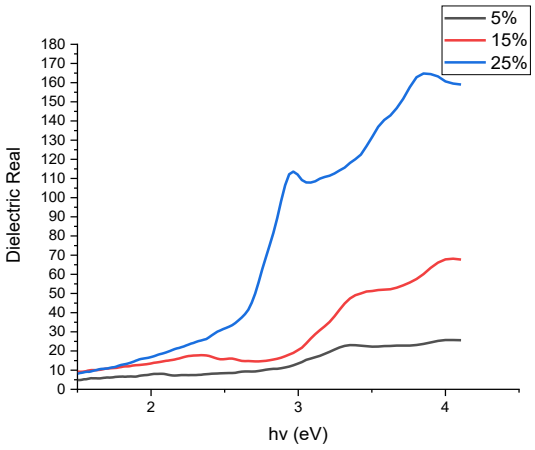

Figure 12. Graph of the dielectric real part against the photon energy for ZnO-TiO_2nanofibre

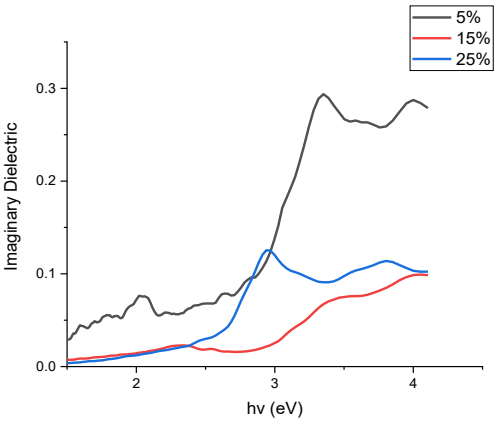

Figure 13. Graph of the dielectric imaginary part against the photon energy for ZnO-TiO_2 nanofibre

DOI: https://doi.org/10.53704/fujnas.v14i1.980

The optical conductivity of the material was also estimated using Equation 9. The relation between the conductivity and photon energy is given in Figure 14

$$Conductivity = \frac{\alpha nc}{4\pi} \qquad 9$$

where n, c and α are the refractive index, speed of light, and absorption coefficient, respectively.

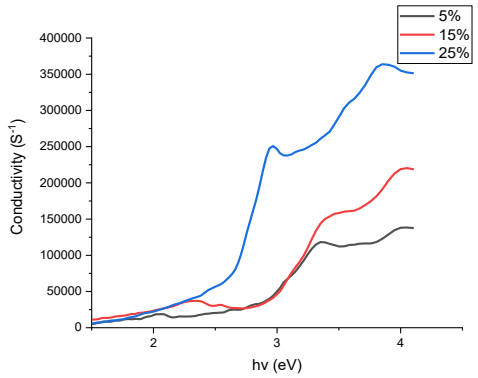

Figure 14: Optical conductivity plot for the ZnO-TiO2 nanofibre

Discussion

The sample exhibited a non-woven nanofibrous morphological structure with an average diameter of 250 nm. The non-woven fibrous structure depicted well-spread, wide pores, which have been reported to enhance photocatalytic degradation of dangerous pollutants and excellent electrolyte soaking in energy conversion and storage devices [22, 23, 24]. The EDS revealed the presence of all the target elements, thereby confirming the successful growth of the composite fibre.

The RBS spectra exhibited little to no traces of contaminants from the organic ingredient, such as acetate, carbon or chlorine from the precursor salt utilised. The peaks primarily represent the metal oxide deposited. Additionally, the spectra of the composite semiconductor oxides showed that the peaks corresponding to Zn and Ti are distinct. This is mainly due to the element's mass difference with the nuclei of the targeted atom, such as zinc, tin, and titanium [25].

The peaks at 2θ angles of 31.78 °, 34.46 °, and 47.25°, with corresponding Miller indices (100), (002), and (110), respectively, matched the ZnO phases in the ZnO-TiO_2 composite. The corresponding diffraction peak for TiO_2 in the ZnO-TiO_2 phase shows major characteristic peaks at 101 (35.46 °), 220 (53.92 °), and 301 (73.78 °), with the most pronounced peak at 101. No 2θ shift was observed for the ZnO phase in the ZnO-TiO_2 composite, which suggests that there is no interaction between the Zn and Ti atoms in the ZnO-TiO_2 phase; as such, ZnO and TiO_2 retained their structural characteristics. The TiO_2 have a rutile tetragonal structure with lattice parameters a= 4.6230 Å, c= 2.9860 Å, and a density of 4.157 g/cm^3 (COD-96-900-4145). The calculated crystallite size was 24.27 nm, and the lattice strain was 0.0023.

A decrease in the transmittance is observed from 5% Ti to 25% Ti in the wavelength region between 400 and 735 nm. The cut-off wavelength shifts from the UV to the visible region with increasing titanium concentration. This suggests that Ti could be used to narrow the bandgap of ZnO into the visible-light frequency range. The absorbance graph (Figure 6) shows a red shift in the absorption edge from 5% Ti to 25% Ti, from 476 to 516 nm. This shows that the optical absorption edge of the electrospun ZnO-TiO_2 nanocomposites fibres demonstrates the displacement of the band edge absorption into the visible region. The observed redshift with the increase in TiO_2 concentration has also been previously reported by [26].

The energy band gap plot of Figure 7 shows that the material exhibited a direct band gap with n = 2, and the band gap reduces with an increase in the TiO_2 concentration. The obtained band gaps for 5%Ti, 15%Ti, and 25%Ti are 2.89, 2.74, and 2.39, respectively. The composite bandgap is lower than the ZnO bandgap reported by [27]. The observed reduction in the band gap of the ZnO-TiO_2 as compared to the ZnO was also reported by [26]. The low value of the optical bandgap in ZnO-TiO_2 nanocomposite compared to ZnO may be attributed to an excessively small particle size of the TiO_2, favouring greater surface defect densities in TiO_2 [28].

From the Urbach analysis, the degree of crystallinity in the ZnO-TiO_2 compound was found to increase as the concentration of Ti increased from 5%Ti to 25%Ti.

The observed higher values of refractive index in the ZnO-TiO_2 electrospun nanofibre composite have been attributed to the composite, which generates new energy levels of TiO_2 and ZnO [29]. The extinction coefficient ranges from 0.001 to 0.029.

Conductivity increases with increasing photon energy and rises significantly around the bandgap, as indicated by the conductivity plot. Similar trends are evident in both the conductivity and dielectric graphs. A strong photon-electron interaction is responsible for the dramatic increase in conductivity and dielectric

DOI: https://doi.org/10.53704/fujnas.v14i1.980

constant near the bandgap. With the real component value being higher than the imaginary, the dielectric properties of the real and imaginary components exhibit the same pattern.

Conclusion

The optical and structural properties of electrospun ZnO–TiO_2 nanofibrous composites were systematically investigated. Increasing TiO_2 concentration narrowed the bandgap from 2.89 eV to 2.39 eV and reduced structural disorder, improving their suitability for visible-light photocatalysis.

Funding

No funding was received for this work

Conflict of Interest

The authors declare no conflict of interest

References

1. Myndrul V, Vysloužilová L, Klápšťová A, Coy E, Jancelewicz M, Balme S. Formation and photoluminescence properties of ZnO nanoparticles on electrospun nanofibers produced by atomic layer deposition. *Coatings*. 2020;12(10):1199.
2. Kurniawan YL, Yuliati L. Activity enhancement of P25 titanium dioxide by zinc oxide for photocatalytic phenol degradation. *Bull Chem React Eng Catal*. 2021;16(2):310–319.
3. Bolarinwa HS, Onuu MU, Animasahun LO, Alayande SO, Fasasi AY. Effect of tin on bandgap narrowing and optical properties of ZnO–Zn_2SnO_4 electrospun nanofibre composite. *J Taibah Univ Sci*. 2020;14(1):1251–1261.
4. Factori I, Amaral J, Camani P, Rosa D, Lima B, Brocchi M. ZnO nanoparticle/poly(vinyl alcohol) nanocomposites via microwave-assisted sol–gel synthesis for structural materials, UV shielding, and antimicrobial activity. *ACS Appl Nano Mater*. 2021;7(4):7371–7383.
5. Lin R, Amrute A, Pérez-Ramírez J. Halogen-mediated conversion of hydrocarbons to commodities. *Chem Rev*. 2017;117(5):4182–4247.
6. Al-Abduljabbar A, Farooq I. Electrospun polymer nanofibers: processing, properties, and applications. *Polymers (Basel)*. 2023;15(1):65.
7. Mustapha S, Ndamitso MM, Abdulkareem AS, Tijani JO, Shuaib DT, Ajala AO, et al. Application of TiO_2 and ZnO nanoparticles immobilized on clay in wastewater treatment: a review. *Appl Water Sci*. 2020;10:49.
8. El-Ramady H, El-Henawy A, Amer M, Omara A, Elsakhawy T, Salama A. Agro-pollutants and their nano-remediation from soil and water: a mini-review. *Environ Sci Proc*. 2020;4:361–375.
9. Lee C, Na K, Kim W, Park D, Yang W, Choi W. TiO_2/ZnO nanofibers prepared by electrospinning and their photocatalytic degradation of methylene blue compared with TiO_2 nanofibers. *Appl Sci*. 2019;9(16):3404.
10. Jiang D, Zhang Q, Chen C. Photocatalytic degradation characteristics of different organic compounds at TiO_2 nanoporous film electrodes with mixed anatase/rutile phases. *Environ Sci Technol*. 2006;41(1):303–308.
11. Eddy DP, Permana MD, Sakti LK, Sheha GA, Solihudin, Hidayat S, et al. Heterophase polymorph of TiO_2 (anatase, rutile, brookite, TiO_2(B)) for efficient photocatalyst: fabrication and activity. *Nanomaterials (Basel)*. 2023;13(4):704.
12. Mahy J, Lambert S, Tilkin R, Wolfs C, Poelman D, Devred F, Douven S. Ambient temperature ZrO_2-doped TiO_2 crystalline photocatalysts: highly efficient powders and films for water depollution. *Mater Today Energy*. 2019;13:312–322.
13. Ferreira S, Rovisco A, Santos A, Águas H, Igreja R, Barquinha P, Martins R. Porous ZnO nanostructures synthesized by microwave hydrothermal method for energy harvesting applications. 2021.
14. Gupta P, Maurya S, Pandey NK, Verma V. Metal-oxide-based ammonia gas sensors: a review. *Nanoscience Nanotechnology-Asia*. 2021;11(3):270–289.
15. Animasahun LO, Taleatu BA, Adewinbi SA, Bolarinwa HS, Fasasi AY. Synthesis of SnO_2/CuO/SnO_2 multilayered structure for photoabsorption: compositional and interfacial structural studies. *J Niger Soc Phys Sci*. 2021;3:74–81.
16. Rütten M, Geilen A, Sebastian A, Krebs D, Salinga M. Localised states and their capture characteristics in amorphous phase-change materials. *Sci Rep*. 2019;9:6592.
17. Böer K, Pohl UW. Defects in amorphous and organic semiconductors. *Semicond Phys*. 2022:1–35.
18. Guimarães NE, Ximenes ERB, da Silva LA. Electrical and optical properties of poly(vinyl chloride)/ZnS nanocomposites. *Mater Res*. 2023;26:e202300xx.
19. Zhang Q, Tan Y, Ren G, Tang T. Ray tracing method of gradient refractive index medium based on refractive index step. *Appl Sci*. 2021;11(3):xxx.
20. Aydogun S, Sendil O, Cobal MB. Optical properties of ZnO thin films by spray pyrolysis technique. *Chin J Phys*. 2012;50:xxx–xxx.
21. Animasahun LO, Taleatu BA, Bolarinwa HS, Fasasi AY, Eleruja MA, Obiajunwa EI, Pelemo DA. Spray pyrolysis deposition and characterisation of dielectric SnO_2 thin films. *Fountain J Nat Appl Sci*. 2019;8(2):11–20.
22. Xu Y, Yuan T, Bian Z, Sun H, Pang Y, Peng C, et al. Electrospun flexible Si/C@CNF nonwoven anode for high-capacity and durable lithium-ion batteries. *Compos Commun*. 2019;11:1–5.
23. Wang L, Li Y, Han P. Electrospinning preparation of g-C_3N_4/Nb_2O_5 nanofiber heterojunction for enhanced photocatalytic degradation of organic pollutants in water. *Sci Rep*. 2021.

DOI: https://doi.org/10.53704/fujnas.v14i1.980

24. Cao X, Chen W, Zhao P, Yang Y, Yu DG. Electrospun porous nanofibers: pore-forming mechanisms and applications for photocatalytic degradation of organic pollutants in wastewater. *Polymers (Basel)*. 2022;14(19):3990.
25. Adeoye AE, Ajenifuja E, Taleatu BA, Fasasi AY. Rutherford backscattering spectrometry analysis and structural properties of thin films deposited by chemical spray pyrolysis. *J Mater*. 2015;2015:2015210.
26. Sridevi KP, Sivakumar S, Sangeetha B, Saravanan K, Praveen H. ZnO–TiO_2 nanocomposites synthesized by sol–gel route: structural and optical properties. *Nat Volatiles Essent Oils*. 2021;8(5):4840–4853.
27. Bolarinwa HS, Onuu MU, Fasasi AY, Alayande SO, Animasahun LO, Abdulsalami IO, et al. Determination of optical parameters of zinc oxide nanofibre deposited by electrospinning technique. *J Taibah Univ Sci*. 2017;11:1245–1258.
28. Bai N, Liu X, Li Z, Ke X, Zhang K, Wu Q. High-efficiency TiO_2/ZnO nanocomposite photocatalysts prepared by sol–gel and hydrothermal methods. *J Sol-Gel Sci Technol*. 2021;99:92–100.
29. Yar A, Haspulat B, Üstün T, Eskizeybek V, Avcı A, Kamış H, Achour S. Electrospun TiO_2/ZnO/PAN hybrid nanofiber membranes with efficient photocatalytic activity. *RSC Adv*. 2017;7:29806–29814.

DOI: https://doi.org/10.53704/fujnas.v14i1.980